Direct Calculation of the Temperature Dependence of 2D-IR Spectra. Urea in Water

Ashley K. Borkowski, N. Ian Campbell, a) and Ward H. Thompson Department of Chemistry, University of Kansas, Lawrence, KS 66045, USA

(Dated: 20 May 2023)

A method for directly calculating the temperature derivative of two-dimensional infrared (2D-IR) spectra from simulations at a single temperature is presented. The approach is demonstrated by application to the OD stretching spectrum of isotopically dilute aqueous (HOD in $\rm H_2O$) solutions of urea as a function of concentration. Urea is an important osmolyte because of its ability to denature proteins, which has motivated significant interest in its effect on the structure and dynamics of water. The present results show that the temperature dependence of both the linear IR and 2D-IR spectra, which report on the underlying energetic driving forces, are more sensitive to urea concentration than the spectra themselves. Additional physical insight is provided by calculation of the contributions to the temperature derivative from different interactions, e.g., water-water, water-urea, and urea-urea, present in the system. Finally, it is demonstrated how 2D-IR spectra at other temperatures can be obtained from only room temperature simulations.

I. INTRODUCTION

Since its development by Hamm, Lim, Hochstrasser in 1998, two-dimensional infrared (2D-IR) spectroscopy has become a powerful technique for investigating molecular structure and dynamics with subpicosecond resolution.^{2–9} Moreover, new advances continue to expand its utility. Here we address one area ripe for development: The effect of temperature on the spectrum. There have been relatively few studies of the temperature dependence of 2D-IR spectra, ^{10–13} despite the fact that they can reveal the driving forces underlying the structural and dynamical properties being probed. In this Paper, we present a method for directly calculating the temperature derivative of the 2D-IR spectrum from simulations at a single temperature. This is an application of the recently developed fluctuation theory for dynamics approach. 14-17 We illustrate the method in a detailed examination of the temperature (and concentration) dependence of the spectra of the OD stretch in aqueous urea solutions. A key finding is that the temperature derivative of the 2D-IR spectra are more sensitive to urea than the spectra themselves.

Osmolytes are often characterized as stabilizers that allow living cells to adjust their osmotic pressure and maintain cell volume. $^{18-23}$ However, urea, shown in Fig. 1, is an osmolyte that denatures proteins and counteracts the properties of other osmolytes, *e.g.*, trimethylamine *N*-oxide (TMAO). $^{18-26}$ For this reason, urea has been studied extensively to understand the origins of these behaviors.

The direct interactions between urea and proteins have been examined in the context of protein stability. $^{27-34}$ Using a transfer model to predict protein folding/unfolding

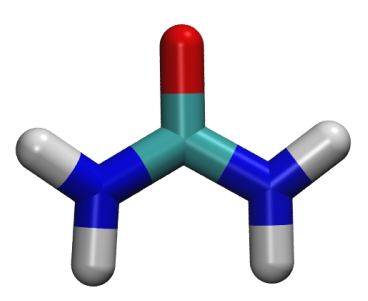


FIG. 1: Stick model of urea. O (red), C (cyan), N (blue), and H (white).

free-energy changes, Bolen and co-workers^{27,28} demonstrate that urea interacts with the protein's backbone and side chains, with the former being larger in magnitude. The interaction of urea with amino acids has also been studied, and it was discovered that urea solvates nonpolar and aromatic residues in addition to the peptide backbone.^{29–31} These findings suggest that urea weakens the hydrophobic effect in proteins, thereby promoting protein unfolding through its interactions with the protein's hydrophobic core.^{30,31} For example, molecular dynamics (MD) simulations of the protein chymotrypsin inhibitor 2 in the presence of urea found that urea promotes protein unfolding both directly, by interacting with the the peptide groups, and indirectly, by altering water structure and dynamics.³⁴

The possibility of such an indirect mechanism of urea for protein denaturation has motivated extensive studies of the influence of urea on water structure using both experiments^{23,24,35-40} and simulations.^{22-25,35,41,42} In this context, a key question is: Does urea act as a "structure-maker" or "structure-breaker," in the same way in which salts are categorized⁴³⁻⁵⁵ according to the Hofmeister series? Due to its ability to denature proteins, it is often grouped with ions that are ranked as more chaotropic, or structure-breaking.⁵⁶ However, Liao et al.

a) Current address: Department of Chemistry, Hendrix College, Conway, AR 72032

b) Electronic mail: wthompson@ku.edu

have argued against the notion that osmolytes indirectly stabilize proteins by altering water structure. ²⁶ Zetterholm $et~al.^{21}$ concluded, based on Raman spectroscopy, that urea destabilizes water structure to promote protein denaturation, while Sahle $et~al.^{23}$ and Yoshida $et~al.^{57}$ observed that urea slightly strengthened the water structure. Many studies indicate that urea is not straightforwardly characterized in this way because it has weak interactions with water. ^{20,35–39,42,58} One argument in this vein postulates that urea is commensurate with water's tetrahedral structure. ^{25,37}

Both linear and nonlinear vibrational spectroscopy of the urea in water system have been used by multiple groups to probe these questions. 21,24,35,36,38,41,58 Carr et al. considered the spectroscopy and dynamics of urea in HOD in $\rm H_2O$ up to 8 M, probing the water OD and urea CO stretches. 24 They reported measurements of the linear IR spectra and simulations of the linear and two-dimensional IR spectra as well as the reorientational dynamics. They found that the OD stretch IR spectrum is insensitive to the urea concentration, which had been previously observed by Sharp et al., 35 while the urea CO stretch blueshifts modestly as urea is added. These results lead them to conclude that urea has a minimal effect on the water structure and should not be considered either a structure-maker or structure-breaker.

They did, however, observe more significant effects of urea on the water dynamics as probed by both the OD stretch anisotropy decay and spectral diffusion. Rezus and Bakker had earlier measured the OD reorientational dynamics in IR pump-probe anisotropy experiments.³⁸ They found the anisotropy decay, as urea is added, maintains a dominant component with the neat water timescale of 2.5 ps, but a smaller component grows in with a timescale too long to be resolved in the experiments. They attributed the slower dynamics to waters that are "immobilized" by engaging in two hydrogen bonds with urea. However, Carr et al., while finding the same slower reorientational dynamics in their simulations, did not observe slower dynamics in such doubly hydrogen-bonded water molecules.²⁴ Instead they attribute the slower reorientational dynamics to an excluded volume effect of the urea molecules, which prevent the approach of new hydrogen-bond partners for water.⁵⁹

In this work, we examine the driving forces underlying the urea-induced changes in the OD stretch 2D-IR spectra in isotopically dilute water. Specifically, the temperature derivatives of both the linear IR and 2D-IR spectra are determined using the developed fluctuation theory approach. These derivatives give insight into the energetic driving forces that determine the spectra. In addition, the method enables calculation of the contributions to the temperature derivative from the different motions and interactions present in the system (e.g., kinetic, Lennard-Jones, and Coulombic energies or waterwater, water-urea, and urea-urea interactions) providing otherwise unavailable mechanistic insight.

II. THEORY

A. General Framework

We have recently shown how the derivative of virtually any dynamical property with respect to temperature or, more precisely, $\beta=1/k_BT$, can be obtained from simulations at a single temperature. The approach is fluctuation theory^{60,61} applied to dynamics¹⁵ and can be illustrated in a general way by considering the statistical mechanical average of a dynamical property, e.g., a time correlation function (TCF) of the form A(0) B(t). In the canonical ensemble,

$$\langle A(0) B(t) \rangle = \frac{1}{h^F Q(\beta)} \int d\mathbf{p} \int d\mathbf{q} \, e^{-\beta H(\mathbf{p}, \mathbf{q})}$$

$$\times A(\mathbf{p}, \mathbf{q}; 0) B(\mathbf{p}, \mathbf{q}; t), \tag{1}$$

where h is Planck's constant, F the number of degreesof-freedom, Q the canonical partition function, and Hthe system Hamiltonian that depends on the full set of momenta (**p**) and coordinates (**q**). Noting that β only appears in the Boltzmann weighting and its normalizing partition function, it is straightforward to show that

$$\begin{split} \frac{\partial \langle A(0) \, B(t) \rangle}{\partial \beta} &= -\frac{1}{Q} \, \frac{\partial Q}{\partial \beta} \, \langle A(0) \, B(t) \rangle \\ &- \frac{1}{h^F \, Q(\beta)} \int d\mathbf{p} \int d\mathbf{q} \, e^{-\beta H(\mathbf{p}, \mathbf{q})} \, H(\mathbf{p}, \mathbf{q}; 0) \\ &\times A(\mathbf{p}, \mathbf{q}; 0) \, B(\mathbf{p}, \mathbf{q}; t). \end{split} \tag{2}$$

Noting, however, that $-\partial \ln Q/\partial \beta = \langle H \rangle$ and that H in the second term is evaluated at time 0, we can define the fluctuation in the system Hamiltonian at t=0 as $\delta H(0)=H(0)-\langle H \rangle$. Then the derivative can be written as

$$\begin{split} \frac{\partial \langle A(0) \, B(t) \rangle}{\partial \beta} &= -\frac{1}{h^F \, Q(\beta)} \int d\mathbf{p} \int d\mathbf{q} \, e^{-\beta H(\mathbf{p}, \mathbf{q})} \\ &\times \delta H(\mathbf{p}, \mathbf{q}; 0) A(\mathbf{p}, \mathbf{q}; 0) \, B(\mathbf{p}, \mathbf{q}; t) \\ &= -\langle \delta H(0) \, A(0) \, B(t) \rangle. \end{split} \tag{3}$$

In other words, the derivative of any TCF with respect to β (and, hence, temperature) can be obtained from a new time correlation function that is the original TCF weighted by the fluctuation in the system energy at t=0. Of key importance is that Eq. (3) can be calculated from simulations at a single temperature; it is the analytical derivative corresponding to the numerical derivative computed in an Arrhenius analysis.

An additional attraction of this approach is that it can provide otherwise unavailable mechanistic insight into the origin of the changes with temperature and hence the driving forces for the dynamics. This is realized by dividing the fluctuations of the total energy, $\delta H(0)$, into contributions from different energetic components, for example, in the context of typical MD simulations

$$\delta H(0) = \delta K E(0) + \delta V_{Coul}(0) + \delta V_{LJ}(0), \qquad (4)$$

where KE is the kinetic energy and V_{Coul} and V_{LJ} are the Lennard-Jones and Coulombic potential energies, respectively. The β derivative of the TCF, Eq. (3), can then be decomposed as,

$$\frac{\partial \langle A(0) B(t) \rangle}{\partial \beta} = -\langle \delta K E(0) A(0) B(t) \rangle
- \langle \delta V_{LJ}(0) A(0) B(t) \rangle
- \langle \delta V_{Coul}(0) A(0) B(t) \rangle.$$
(5)

This is, however, only one of the simplest possible decompositions. In the context of the water-urea system investigated in this work, we also consider the total system energy fluctuation written as

$$\delta H(0) = \delta K E(0) + \delta V_{w-w}(0) + \delta V_{u-w}(0) + \delta V_{u-u}(0),$$
(6)

where V_{w-w} , V_{u-w} , and V_{u-u} are the components of the potential energy due to water-water, water-urea, and urea-urea interactions, respectively. Each of these terms can be further decomposed into the types of interactions involved, for example,

$$\delta V_{u-w}(0) = \delta V_{u-w,LJ}(0) + \delta V_{u-w,Coul}(0) \tag{7}$$

In the following, we use such decompositions of the derivatives of the linear and nonlinear vibrational spectra to provide important insights into the effects of urea on the water spectrum.

B. Linear IR Spectrum

We recently applied the fluctuation theory approach described in Sec. II A to calculate the temperature derivative of the IR spectrum. ^{16,17} The IR line shape can be calculated from the Fourier transform,

$$I(\omega) = \frac{1}{2\pi} \int_{-\infty}^{\infty} e^{-i\omega t} \phi(t) dt$$
 (8)

of the dipole-dipole response function,

$$\phi(t) = \left\langle \vec{\mu}_{01}(0) \cdot \vec{\mu}_{01}(t) e^{i \int_0^t \omega_{01}(\tau) d\tau} \right\rangle e^{-|t|/2T_1}.$$
 (9)

Here, $\vec{\mu}_{01}(t) = \langle 1|\hat{\mu}|0\rangle = \mu_{01}(t)\,\vec{e}(t)$ is the matrix element of the transition dipole moment vector for the mode of interest at time t, $\omega_{01}(t)$ is the $0 \to 1$ vibrational frequency gap at time t, and T_1 is the n=1 vibrational relaxation lifetime. Then the derivative of the dipole-dipole response function with respect to β results in the following expression:¹⁶

$$\frac{d\phi(t)}{d\beta} = -\left\langle \delta H(0) \,\vec{\mu}_{01}(0) \cdot \vec{\mu}_{01}(t) e^{i \int_0^t \omega_{01}(\tau) \, d\tau} \right\rangle
\times e^{-|t|/2T_1}
= -\phi_H(t).$$
(10)

Here, we have neglected any temperature dependence of the relaxation time T_1 , though this could be straightforwardly included. Experimental reports indicate T_1 increases with temperature for HOD in $\rm H_2O$, but only weakly, 12,62 and is essentially independent of urea concentration, 38 indicating it should have a minor effect on the temperature dependence of the spectra.

In the notation of Eq. (8), the temperature derivative of the IR spectrum is then,

$$\frac{dI(\omega)}{d\beta} = -\frac{1}{2\pi} \int_{-\infty}^{\infty} e^{-i\omega t} \phi_H(t) dt, \qquad (11)$$

i.e., the negative of the Fourier transform of this weighted response function, $\phi_H(t)$. Note that this derivative can be calculated from the same, single temperature, simulations as $I(\omega)$ itself.

C. 2D-IR Spectrum

The 2D-IR spectrum can be obtained in an analogous, if more complicated, fashion than the linear IR spectrum. Following the approach of Skinner and co-workers, ^{63,64} the heterodyne-detected signal is given by the double-Fourier transform of rephasing and non-rephasing TCFs,

$$I_{2DIR}(\omega_{1}, \omega_{3}; T_{w}) = \operatorname{Re} \left\{ \int_{0}^{\infty} dt_{3} e^{i\omega_{3}t_{3}} \int_{0}^{\infty} dt_{1} \left[R_{r}(t_{1}, T_{w}, t_{3}) e^{-i\omega_{1}t_{1}} + R_{nr}(t_{1}, T_{w}, t_{3}) e^{i\omega_{1}t_{1}} \right] \right\}. \quad (12)$$

Here, ω_1 and ω_3 are the pump and probe frequencies and T_w is the waiting time. The rephasing and non-rephasing contributions are each the sum of three TCFs:

$$R_r(t_1, T_w, t_3) = \sum_{j=1}^{3} R_j(t_1, T_w, t_3)$$
 (13)

and

$$R_{nr}(t_1, T_w, t_3) = \sum_{j=4}^{6} R_j(t_1, T_w, t_3), \tag{14}$$

which are of the form, for example,

$$R_{1}(t_{1}, T_{w}, t_{3}) = \left\langle \mu_{01}(0) \,\mu_{01}(t_{1}) \,\mu_{01}(t_{1} + T_{w}) \right.$$

$$\mu_{01}(t_{1} + T_{w} + t_{3}) \,e^{\int_{0}^{t_{1}} \,\omega_{01}(\tau)d\tau}$$

$$e^{-\int_{t_{1} + T_{w}}^{t_{1} + T_{w} + t_{3}} \,\omega_{01}(\tau)d\tau} \right\rangle \,e^{-T_{w}/T_{1}}, \quad (15)$$

Additional details and the other five TCFs are given in the Appendix.

In this Paper, we show how the same fluctuation theory described above can be used to directly calculate the temperature derivative of the 2D-IR spectrum. The approach is that described in Sec. II A. The TCFs that yield the 2D-IR spectrum depend on temperature only through the Boltzmann weighting of the thermal average that appears as a factor of $e^{-\beta H}$ inside the the average and a factor of 1/Q outside it. Then, for example, the derivative of the R_1 TCF with respect to β follows the result in Eq. (3):

$$\frac{\partial R_1(t_1, T_w, t_3)}{\partial \beta} = -\left\langle \delta H(0) \,\mu_{01}(0) \,\mu_{01}(t_1) \,\mu_{01}(t_1 + T_w) \right.$$

$$\mu_{01}(t_1 + T_w + t_3) \,e^{\int_0^{t_1} \omega_{01}(\tau)d\tau}$$

$$e^{-\int_{t_1 + T_w}^{t_1 + T_w + t_3} \omega_{01}(\tau)d\tau} \right\rangle e^{-T_w/T_1}$$

$$\equiv -R_{1,H}(t_1, T_w, t_3). \tag{16}$$

With analogous derivatives for the other five TCFs, which are given in the Appendix, we can obtain the corresponding derivatives of the rephasing and non-rephasing contributions,

$$\frac{\partial R_r(t_1, T_w, t_3)}{\partial \beta} = -\sum_{j=1}^3 R_{j,H}(t_1, T_w, t_3)$$

$$\equiv -R_{r,H}(t_1, T_w, t_3) \tag{17}$$

and

$$\frac{\partial R_{nr}(t_1, T_w, t_3)}{\partial \beta} = -\sum_{j=4}^{6} R_{j,H}(t_1, T_w, t_3),$$

$$\equiv -R_{nr,H}(t_1, T_w, t_3) \tag{18}$$

Then, the derivative of the 2D-IR spectrum is given by

$$\frac{\partial I_{2DIR}(\omega_1, \omega_3; T_w)}{\partial \beta} = -\operatorname{Re}\left\{ \int_0^\infty dt_3 \, e^{i\omega_3 t_3} \int_0^\infty dt_1 \right. \\
\left. \left[R_{r,H}(t_1, T_w, t_3) \, e^{-i\omega_1 t_1} \right. \right. \\
\left. + R_{nr,H}(t_1, T_w, t_3) \, e^{i\omega_1 t_1} \right] \right\}. \tag{19}$$

This result has a couple of important features. First, this temperature derivative can be obtained from simulations at a single temperature; the same simulations can be used to compute both I_{2DIR} and its temperature (or β) derivative. Second, the decompositions of the fluctuation of the total energy, e.g., as shown in Eqs. (4)-(7), can be used in the expressions for the $R_{j,H}$ to yield contributions to $\partial I_{2DIR}/\partial\beta$ from the different motions and interactions present in the system. This is mechanistic information for the 2D-IR spectra that cannot be obtained in any other way.

III. COMPUTATIONAL METHODS

A. Molecular Dynamics

All MD simulations were performed using the Large-Scale Atomic/Molecular Massively Parallel Simulator

(LAMMPS). 65,66 Each simulation consisted of SPC/E water molecules, ⁶⁷ and urea molecules described by the Kirkwood-Buff force field (KBFF)⁶⁸ to form concentrations of approximately 1, 4 and 8 M. The intermolecular force field parameters for each atom are provided in Table S1 and the bonded parameters for the urea molecules are given in Table S2. Each urea system was first equilibrated for 1 ns and then propagated for 25 ns at constant pressure and temperature using an NpT ensemble at 1 bar and 298.15 K, with a Nosé-Hoover thermostat and barostat using pressure and temperature chain lengths of three. The damping parameters for the barostat and the thermostat were 1000 and 100 fs, respectively. The latter stage was used to determine the average volume that was used in subsequent NVT ensemble simulations. The differences in average volume give rise to small deviations from the nominal 1, 4, and 8 M concentrations; the precise values are given in Table S3.

Based on the calculated equilibrium volume, a constant volume and temperature simulation for each urea system was run for a 1 ns equilibration and 5 ns run stages at 298.15 K. A Nosé-Hoover thermostat using the same parameters given above was used. During the latter, the configurations and momenta were written every 1 ps. These were used as the initial conditions for 5000 NVE trajectories of 10 ps length from which the configurations were saved every 5 fs. The linear IR and 2D-IR spectra were computed from these NVE trajectories, an approach that eliminates any effect of the thermostat on the dynamics. For neat HOD in $\rm H_2O$, five separate trajectories at a density of 1.00 g/cm³ were run with 0.5 ns equilibration and 1 ns run stages; the other simulation details are the same as for the urea systems.

In every simulation, the time step was 1 fs, the SHAKE algorithm was used for the bonds and angles of each water molecule along with the O-C and N-H bonds within each urea molecule, and the electrostatics were calculated using the particle-particle particle-mesh Ewald summation with an tolerance of 1×10^{-4} . Errors in the computed results were obtained by block averaging using 5 blocks (each block representing 1000 NVE trajectories) and are reported as 95% confidence intervals using the Student's t-distribution.⁶⁹

B. Empirical Mapping Approach

The spectra presented in this work are calculated using the empirical, or electrostatic, mapping approach that approximates the quantum mechanical vibrational frequencies and transition dipole moments from information directly available in a classical MD simulation.^{24,70–73} Specifically, each quantity is written in terms of an empirical relationship obtained by correlating the results of explicit quantum mechanical calculations on a cluster to the electric fields computed from classical MD models.

For example, the fundamental transition frequency is obtained as $\omega_{01} = c_0 + c_1 \mathcal{E} + c_2 \mathcal{E}^2$, where \mathcal{E} is the (classical

MD) electric field component along the OD bond evaluated at the D atom position and c_0 , c_1 , and c_2 are constants. The constants used in this work for the transition frequencies (ω_{01} and ω_{12}) as well as the dipole derivative (μ') and coordinate matrix elements (x_{01} and x_{12}) used to compute the transition dipoles (μ_{01} and μ_{12}) are taken from Ref. 24 and are given in Table S4.

IV. RESULTS

A. Linear IR Spectrum and Derivative

It is useful to first consider the OD IR spectrum as a function of urea concentration, which is shown in Fig. 2a. The addition of urea has only minor effects on the spectrum. The 1 M urea solution has a spectrum essentially identical to that of neat water. At higher concentrations, there is little shift in the peak position and slight broadening, primarily on the lower frequency side. This modest influence of urea on the OD spectrum has been previously observed in simulations and measurements. ^{24,36} These results emphasize the weak effect of urea on the water structure as probed through the IR spectrum.

Additional insight is gained by examination of the derivative of the spectrum with respect to inverse temperature, $\partial I(\omega)/\partial \beta$, which is shown for the four solutions in Fig. 2b. The shape of the derivative mirrors what we have observed previously in simulations of the OH stretch spectra of HOD in D₂O, both in the neat liquid¹⁶ and in salt solutions.¹⁷ Namely, $\partial I(\omega)/\partial \beta$ is positive for lower frequencies corresponding to OD groups engaged in stronger H-bonds, but turns negative for higher frequency with weaker H-bonded OD groups. (Here, we refer to the strength of the H-bond as measured by its vibrational frequency, but it is important to acknowledge that there are multiple ways in which H-bond strength can be characterized.) This means that the spectrum will red-shift as T decreases (β increases) favoring strong Hbonds, but blue-shift as T increases. We have shown that this behavior can be understood in terms of competing energetic and entropic driving forces. 16,17

The derivative shows stronger effects of added urea compared to the spectrum itself. Namely, the derivative becomes flatter, *i.e.*, the maximum and minimum values are reduced, as the urea concentration increases, with a more significant effect on the maximum. This is similar to the effect observed when alkali-halide salts are added to water. ¹⁷ In addition, a shoulder in the derivative grows in at lower frequencies, below $\sim 2450~{\rm cm}^{-1}$, indicating that the presence of urea makes those OD groups more energetically favorable.

The contributions to the IR spectrum derivative due to the different interactions present in these systems can also be analyzed as summarized in Eq. (5) and (6). The results are presented in the Supplementary Material, Figs. S1 and S2, but we forgo a detailed discussion of this analysis to focus on the 2D-IR results.

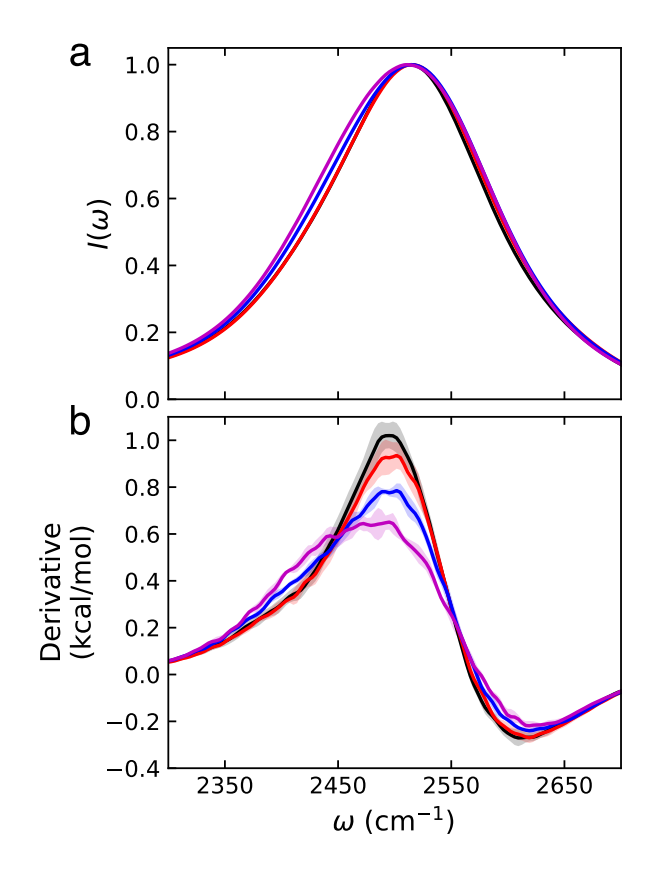


FIG. 2: **a.** HOD in H₂O IR spectra for neat water (black), 1 M (red), 4 M (blue), and 8 M (purple) urea. The spectra are normalized to have a maximum at 1. **b.** The derivative, $\partial I(\omega)/\partial \beta$, of each IR spectrum. Shaded regions show 95% confidence intervals.

B. 2D-IR Spectrum

We now turn to the 2D-IR spectrum of the HOD in H₂O solutions of varying urea concentration. The spectra are shown for 0, 1, 4, and 8 M solutions in Fig. 3. For all cases, a clear evolution of the spectra from a strong correlation between the pump (ω_1) and probe (ω_3) frequencies at zero waiting time to a rounded peak shape at longer T_w can be seen. This is indicative of the loss of memory of vibrational frequency for the OD groups being probed. While this change in the spectra is nearly complete at $T_w = 1$ ps for the neat water case, it persists for longer timescales as urea is added to the solution. In particular, we see only modest differences between the spectra for neat water and the 1 M urea solution. However, at the higher urea concentrations, the correlation of the vibrational frequency is retained for significantly longer times, e.g., even at $T_w = 5$ ps for the 8 M solution.

These vibrational frequency dynamics, or spectral diffusion, can be quantitatively characterized by the centerline slope (CLS) of the spectra as a function of waiting time.⁷⁴ We obtain the center line from the values of ω_3 at the maximum of the positive-going $(0 \to 1)$ peak for each

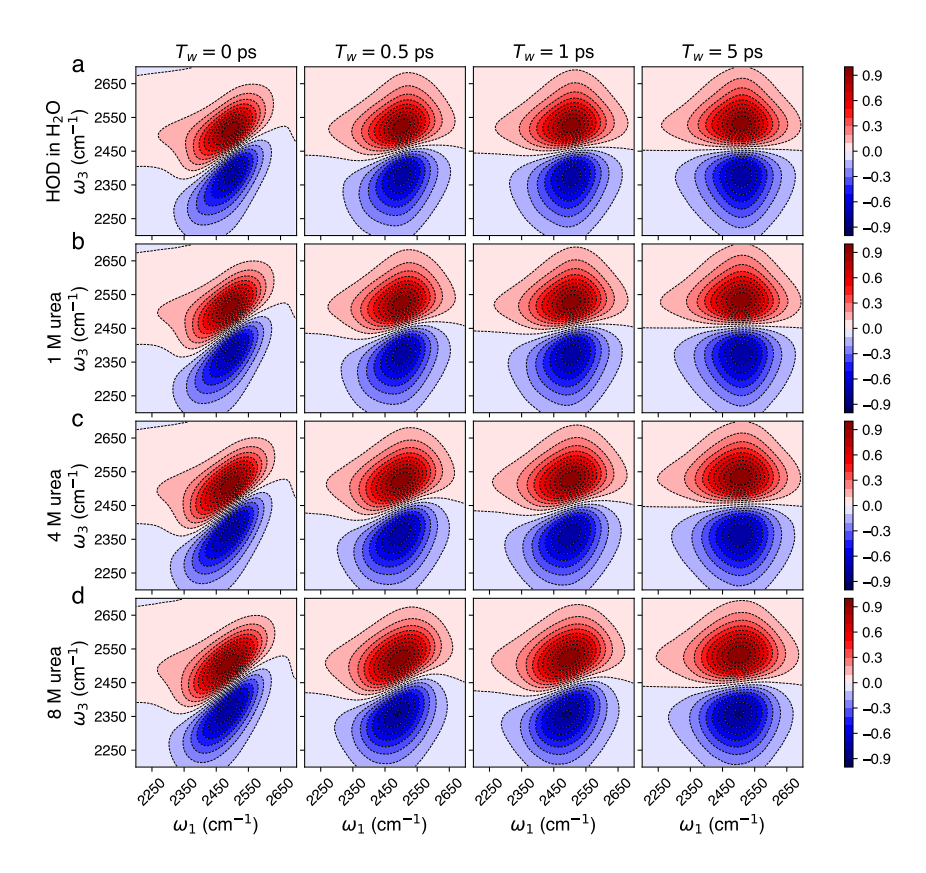


FIG. 3: Simulated OD stretch 2D-IR spectra of $\mathrm{HOD/H_2O}$ as a function of the waiting time, T_w , for **a.** the neat water case and urea solutions of concentration **b.** 1 M, **c.** 4 M, and **d.** 8 M. Each spectrum is normalized so that its maximum equals one.

 ω_1 value. These are determined from a 220 cm⁻¹ wide range of ω_1 values centered at the position of the global maximum of the peak. The CLS is then the slope of this line, which is determined at each waiting time. The results obtained from the present simulations are shown in Fig. 4 as a function of concentration and the CLS values are provided in Table S5.

The CLS decays more slowly as urea is added to the solution. The biggest changes are observed for the 4 and 8 M concentrations, which have both a larger CLS at $T_w=0$ and exhibit slower decays with waiting time. The 0 and 1 M solutions have CLS values that are nearly identical for short waiting times (≤ 1 ps), but the latter shows a slower decay at longer times. Altogether these results indicate that the presence of urea slows water spectral diffusion and this effect grows significantly at higher concentrations. This is consistent with the prior simulations by Carr et al.,²⁴ who reported similar behavior in the 2D-IR nodal slope and attributed it to rigidification of the water network surrounding urea. We explore the driving forces in greater detail below through analysis of the temperature derivatives.

C. Temperature Derivative of the 2D-IR Spectrum

The derivatives of the 2D-IR spectra with respect to β have been calculated using Eq. (19) and are shown in Fig. 5 as a function of urea concentration and waiting time. The corresponding 2D-IR spectra from Fig. 3 are shown as dashed contours to provide context for the derivatives. There are a number of interesting features to note.

We first consider the size of the derivative, which is indicated by the contour scales on the right side of the figure. The magnitude decreases as the urea concentration increases. Quantitatively, the maximum derivative decreases by $0.75-1~\rm kcal/mol$ depending on the waiting time. This is qualitatively the same behavior observed in Fig. 2b, and both results indicate that urea reduces the energy changes associated with changing the OD frequency. However, the magnitude of the derivatives are larger for the 2D-IR spectra, by a factor of $\sim 3-4$.

Examination of the derivative contours in Fig. 5 also reveals that the temperature derivative increases in magnitude with the waiting time. At $T_w = 0$, the maximum in the derivative is $\sim 1 \text{ kcal/mol}$ lower than it is at the longest, $T_w = 5$ ps waiting time. This indicates that the temperature derivative is sensitive to the dynamics governing the 2D-IR spectrum.

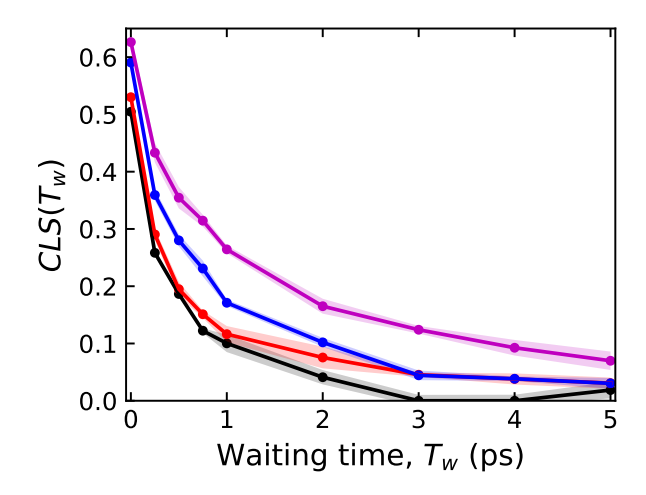


FIG. 4: Center-line slope, $CLS(T_w)$, as a function of the waiting time for the simulated OD stretch 2D-IR spectra of HOD/H₂O for neat water (black), 1 M (red), 4 M (blue), and 8 M (purple) urea solutions. Shaded regions indicate 95% confidence intervals.

A key feature of the 2D-IR spectra derivatives is the difference in the location of the derivative maximum relative to the spectrum maximum. Consider the $T_w=0$ results in Fig. 5 for the positive-going $0 \to 1$ peak that, for all urea concentrations, is positive for lower values of both ω_1 and ω_3 but changes sign at higher frequencies. A diagonal cut through the derivative is qualitatively similar to that of the linear IR spectrum shown in Fig. 2, *i.e.*, both indicate the spectra will redshift as temperature decreases and blueshift as temperature increases; the origins of this behavior is examined in greater detail below. This feature is generally preserved as the waiting time increases.

Finally, the temperature derivatives also are significantly narrower than the 2D-IR spectra themselves. This indicates that changing the temperature leads not only to shifts in the peak position of the spectra, but also in changes to the peak widths. Specifically, the peaks will narrow as temperature decreases (*vide infra*).

V. DISCUSSION

We now turn to a discussion of the origins and implications of the 2D-IR derivatives presented above. The former are interrogated using the decompositions of the derivative described in Sec. II A with two different approaches. The latter are examined in the context of predictions of the temperature-dependent spectra.

A. Contributions by Interaction Type

The simplest decomposition of the total energy within the MD simulations used in this work is given by Eq. (4). We now consider the contribution of each of these terms to the temperature derivative of the 2D-IR spectrum by using the decomposition in Eq. (19). The results obtained from this analysis are shown as a function of waiting time in Fig. 6 for the 8 M urea solution.

Effectively, these contributions to the derivative are divided by the type of interaction or motion. The most notable feature is that there is a competition between the Lennard-Jones and Coulombic potential energy contributions. Namely, the Coulombic contribution to the derivative shown in Fig. 6d is primarily positive for the $0 \rightarrow 1$ peak, turning negative only at the highest frequencies, but the signs are reversed for the Lennard-Jones contribution in Fig. 6c.

This is a (so-far) universal feature of water structure and dynamics that has been observed for every observable to which we have applied fluctuation theory for dynamics, e.g., the diffusion coefficient, 55,75,76 reorientation time, 75-77 hydrogen-bond exchange time, 78 linear IR spectrum, 16,17 radial distribution function, 79 viscosity, 80 and spectral diffusion time. 81 This behavior reflects the description of the hydrogen bond as driven by the electrostatic attraction of the positively charged, H atom donor and the negatively charged O atom acceptor, which is held in tension by the shorter-ranged Lennard-Jones interaction that holds the two apart. At the close distances of the hydrogen bond, the Coulombic energy is favorable while the Lennard-Jones interaction is largely repulsive, leading to the opposing behavior seen in Fig. 6.

Polarization and charge transfer effects, which must also be present in water, are obviously only described in an averaged way in the fixed charge force fields used here. While we plan to explore these in detail in the future, we have previously examined three-body descriptions and found the same competition between electrostatic and Lennard-Jones interactions observed in three- and four-site fixed charge models. ⁷⁶

It is important to note that the contribution from the Coulombic interactions to the 2D-IR spectrum derivative is significantly larger, by a factor of $\sim 2-3$, than the Lennard-Jones one. This reflects the dominant role of electrostatics in driving the hydrogen-bonded structure of water. Their behavior with waiting time is not the same, however. As T_w increases from 0 to 5 ps, the maximum in the Coulombic contributions grows, from 2.1 to 2.8 kcal/mol, while the Lennard-Jones minimum falls more modestly from -0.9 to -1.0 kcal/mol. This is one reason that the total temperature derivative grows in magnitude with T_w .

The second reason is found in the kinetic energy contribution, shown in Fig. 6b, which also increases with waiting time, from 0.5 to 0.8 kcal/mol. It is noteworthy that this component of the derivative is significantly larger than that found for the linear IR spectrum, for

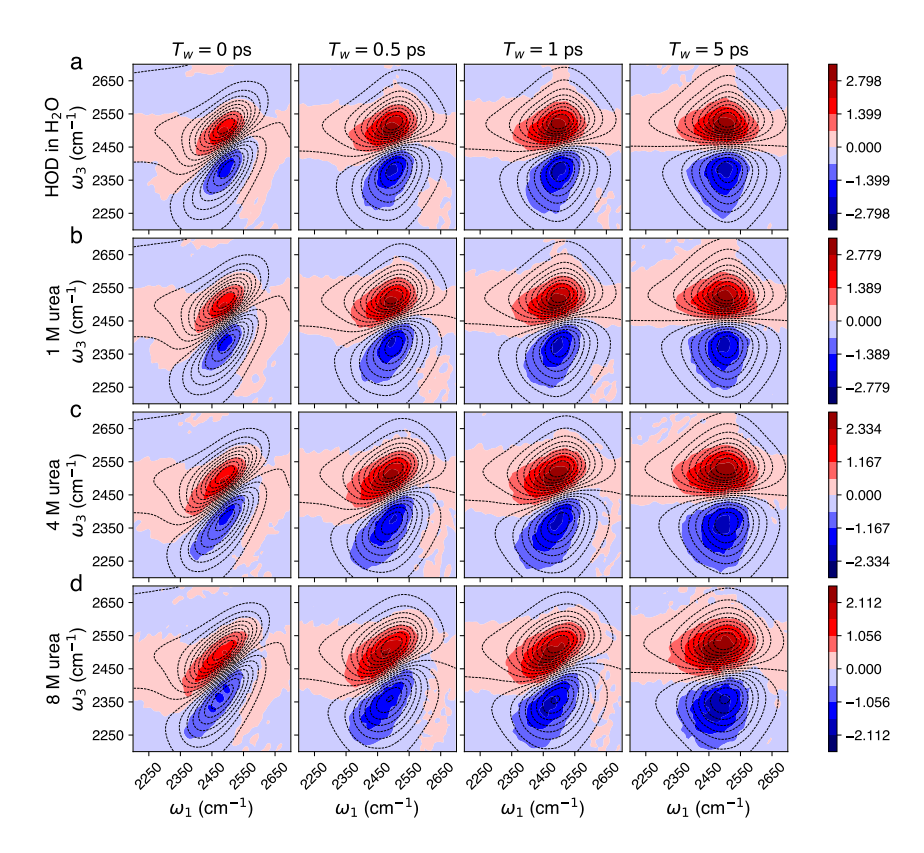


FIG. 5: Calculated derivative (in kcal/mol) of the normalized OD stretch 2D-IR spectra, $\partial I(\omega_1, \omega_3; T_w)/\partial \beta$, of HOD/H₂O as a function of waiting time for **a.** the neat water case and urea solutions of concentration **b.** 1 M, **c.** 4 M, and **d.** 8 M. Black dashed contour lines represent the 2D-IR spectra from Fig. 3.

which it is less than $0.1~\rm kcal/mol$. This is indicative of the greater dependence of the 2D-IR spectrum on the dynamical behavior of the liquid.

The results for 1 and 4 M urea in HOD/H_2O are shown in Figs. S3 and S4 of the Supplementary Material. The primary effect of increasing urea concentration is an increase in the absolute magnitude of the Coulombic and Lennard-Jones contributions. The kinetic energy contribution is more modestly affected by the addition of urea.

B. Intermolecular Interaction Contributions

We next consider the contributions to the temperature derivative from the water-water, water-urea, and ureaurea interactions given by Eqs. (6) and (7). The results obtained from this analysis are shown as a function of waiting time in Fig. 7 for the 8 M urea solution (and the 1 and 4 M urea results are shown in Figs. S5 and S6 of the Supplementary Material). Note that these three contributions do not sum to the total derivative because they do not include kinetic energy contributions.

We first note the qualitative features. Both the water-water and water-urea contributions, shown in Fig. 7b,c, to the derivative are positive over most of the positive-going, $0 \rightarrow 1$, peak of the 2D-IR spectra. The water-

water contributions become negative at larger frequencies, while the water-urea component is positive for all regions of the $0 \to 1$ peak and its maximum is also blueshifted (in both ω_1 and ω_3). In contrast, the urea-urea contribution to the derivative, shown in Fig. 7d, is negative for the $0 \to 1$ peak, with a similar shape (but opposite sign) to the water-urea component. Thus, we see that as temperature is lowered, the water-water interactions tend to redshift and narrow the 2D-IR spectrum, the water-urea interactions tend to narrow the spectrum and increase its amplitude, in competition with an opposing effect from the urea-urea contributions.

The behavior of the water-water interactions is similar to that of the neat HOD in $\rm H_2O$ results shown in Fig. 5a and reflects the behavior seen in the neat water linear IR spectrum (see Fig. 2 and Ref. 16). Namely, as temperature increases, the higher frequency, weaker H-bonds are favored, while lowering temperature shifts the spectrum to the more red-shifted, stronger H-bonds. The 2D-IR derivatives indicate that this effect is increased for longer waiting times. The water-urea contributions to the derivative do not indicate the same shifting of the spectrum with temperature, presumably because of weaker water-urea H-bonds, compared to those between water molecules. The opposite behavior of the urea-urea contributions compared to the water-urea ones are likely

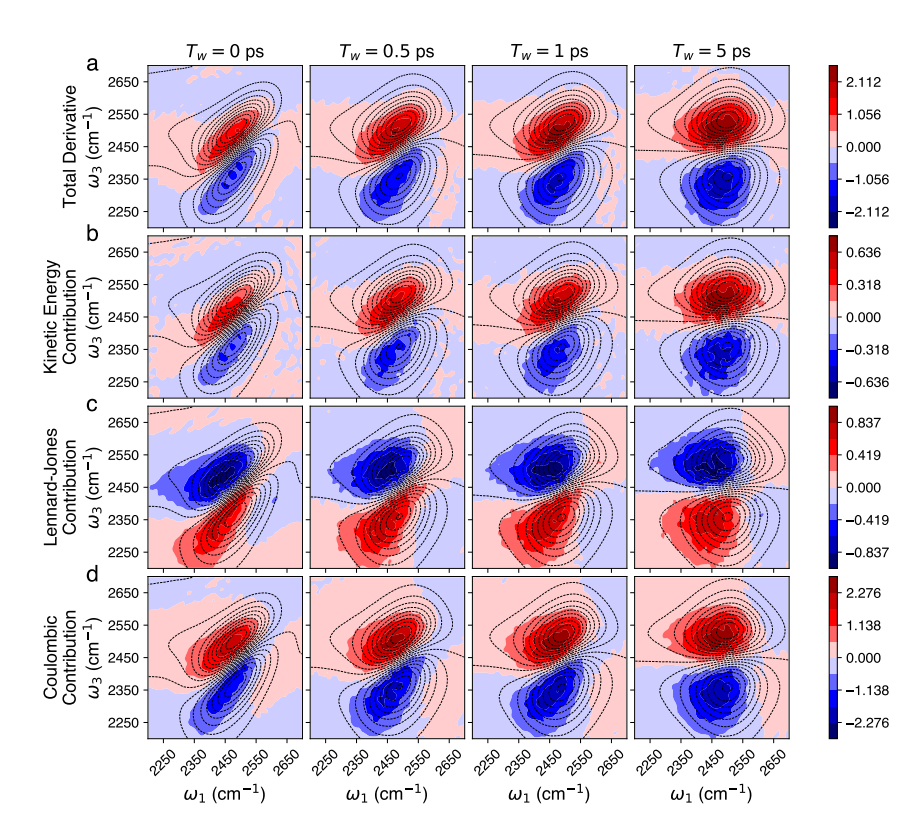


FIG. 6: Contributions to the derivative, $\partial I(\omega_1, \omega_3; T_w)/\partial \beta$, of the simulated OD stretch normalized 2D-IR spectra of 8 M urea in HOD/H₂O as a function of waiting time. Results are shown for the **a**. total derivative and the **b**. kinetic, **c**. Lennard-Jones interaction, and **d**. Coulombic interaction energies. Black dashed lines in each panel show the corresponding 2D-IR spectra.

due to disruption of the water-water and water-urea H-bonding by favorable urea-urea interactions.

The water-water interaction contributions represent the largest component of the derivative, which can be seen by comparing the scales of the contour plots. Like the total derivative, the water-water contribution grows with waiting time, with its maximum value increasing from 1 to 1.6 kcal/mol as T_w increases from 0 to 5 ps. The next largest contribution comes from the water-urea interaction which is less sensitive to the waiting time; its maximum grows from 0.9 to 1 kcal/mol with increasing T_w . The urea-urea interactions counteract these waterurea contributions but with a significantly smaller magnitude. They have a minimum value of $\sim -0.3 \text{ kcal/mol}$ that is essentially independent of T_w . These results thus indicate that the total temperature derivative of the 2D-IR spectra are driven primarily by the water-water and water-urea interactions. However, the latter only modestly affects the qualitative behavior of the temperature derivative.

The effect of increasing urea concentration can be seen by comparing the 8 M results in Fig. 7 to those for the 1 and 4 M solutions in Figs. S5 and S6. The primary result of adding urea is an increase in the absolute magnitude of the water-urea and urea-urea interaction contributions, as more water molecules are influenced by urea, directly and indirectly, at the higher concentrations. These are quite small, almost negligible, for the 1 M solution, but become significant for the 4 M case. Similarly, the waterwater interaction contribution decreases in magnitude from 1 to 4 M, but is relatively constant from 4 to 8 M urea.

C. Temperature Predictions of the 2D-IR Spectrum

A key advantage of calculating the temperature derivative of the spectrum at a single temperature is that it can be used to predict the spectrum at other temperatures. We have previously demonstrated this for the linear IR spectrum. 16,17 In that case, the approach is to treat the spectrum as an effective probability distribution from which an effective free energy is obtained as a function of vibrational frequency. Then the temperature derivative yields the underlying internal energy and entropy as a function of frequency. The former can then be used in a van't Hoff relation to predict the IR spectrum over a wide range of temperatures. The same approach is, however, not straightforwardly applicable to the 2D-IR spectrum which is not positive definite and thus cannot be readily described as an effective probability distribution; it thus remains to develop an analogous

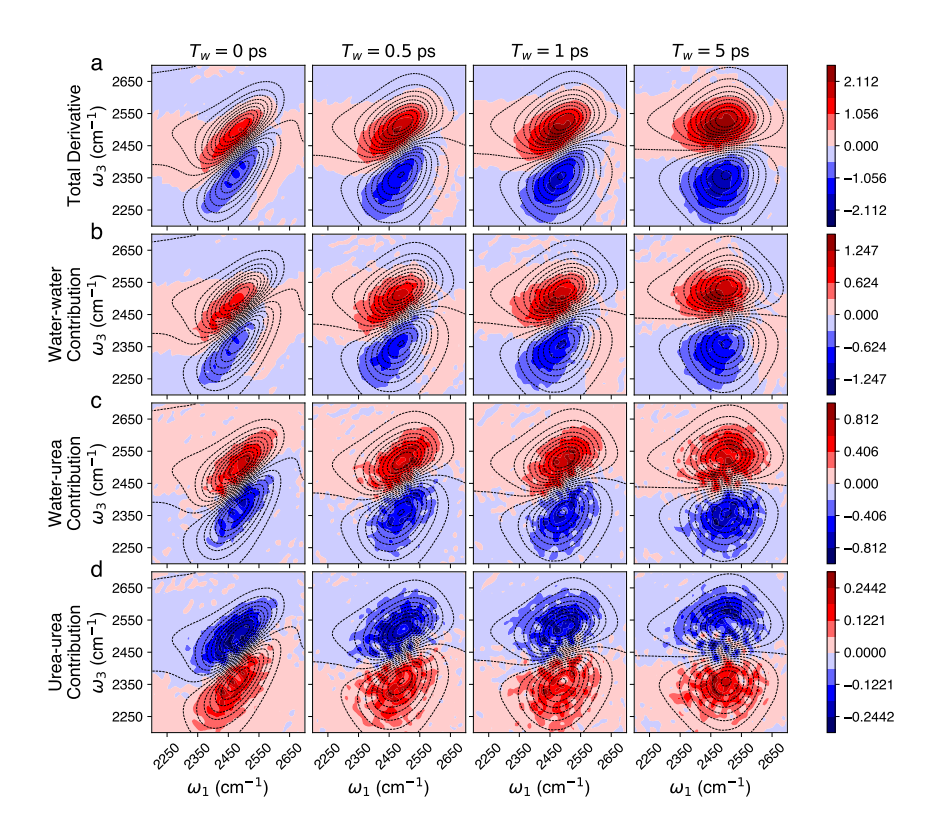


FIG. 7: Contributions to the derivative, $\partial I(\omega_1, \omega_3; T_w)/\partial \beta$, of the simulated OD stretch normalized 2D-IR spectra of 8 M urea in HOD/H₂O as a function of waiting time. Results are shown for the **a**. total derivative and the **b**. water-water, **c**. water-urea, and **d**. urea-urea contributions from the addition of the Lennard-Jones and Coulombic interaction energies. Black dashed lines in each panel show the corresponding 2D-IR spectra.

van't Hoffian description of the 2D-IR spectrum.

For the present, we instead have adopted a simpler, but more local, approximation for predicting the 2D-IR spectrum at other temperatures. Specifically, we have use a simple Taylor series approximation to express the spectrum at a given $\beta = 1/k_BT$ in terms of the spectrum and derivative at a reference $\beta_0 = 1/k_BT_0$:

$$I_{2DIR}^{pred}(\omega_1, \omega_3; T_w)|_{\beta} = I_{2DIR}(\omega_1, \omega_3; T_w)|_{\beta_0} + \frac{\partial I_{2DIR}(\omega_1, \omega_3; T_w)}{\partial \beta} \Big|_{\beta_0} (\beta - \beta_0).$$

$$(20)$$

Note that this is the first-order approximation to a van't Hoff description. As observed for the van't Hoff description of linear IR spectra, these predictions are not naturally norm-preserving, so Eq. (20) should not accurately predict the change in the maximum value of the 2D-IR spectrum. Thus, we constrain our comparisons to normalized spectra.

We have used the Taylor series expansion in Eq. (20) to predict the OD stretch 2D-IR spectra for 8 M urea at 280 K and 320 K from simulations at room temperature. The results are shown in Fig. 8 and compared with direct calculations at the other temperatures using the same simulation approach as described in Sec. III using

 $1~\mathrm{ns}$ equilibration and $1~\mathrm{ns}$ run stages at the respective temperatures to generate the initial conditions for $1000~\mathrm{NVE}$ trajectories.

The Taylor-series predicted 2D-IR spectra for 280 K shown in Fig. 8b are essentially indistinguishable from the directly calculated spectra, Fig. 8a. At this lower temperature, the spectra are redshifted and the peaks are narrowed (in both the diagonal and anti-diagonal directions) compared to the room temperature result. At the same time, the spectral diffusion, as measured by the $CLS(T_w)$ is slower. All of these effects are faithfully captured by the predicted spectra.

At 320 K, the predicted spectra shown in Fig. 8d also describe the significant changes relative to the spectra at room temperature. These are naturally qualitatively opposite to that observed when lowering the temperature: As the temperature is increased the spectra blueshift and broaden while spectral diffusion is accelerated. The agreement between the directly calculated spectra at 320 K and the predictions from the Taylor series expansion is not as quantitative as the 280 K results, with some minor deviations observed at longer waiting times. While the predictions are still accurate, this points to the limitations of the Taylor series description, which is intrinsically local in temperature. This is further illustrated in Fig. S7, where calculated and predicted spectra

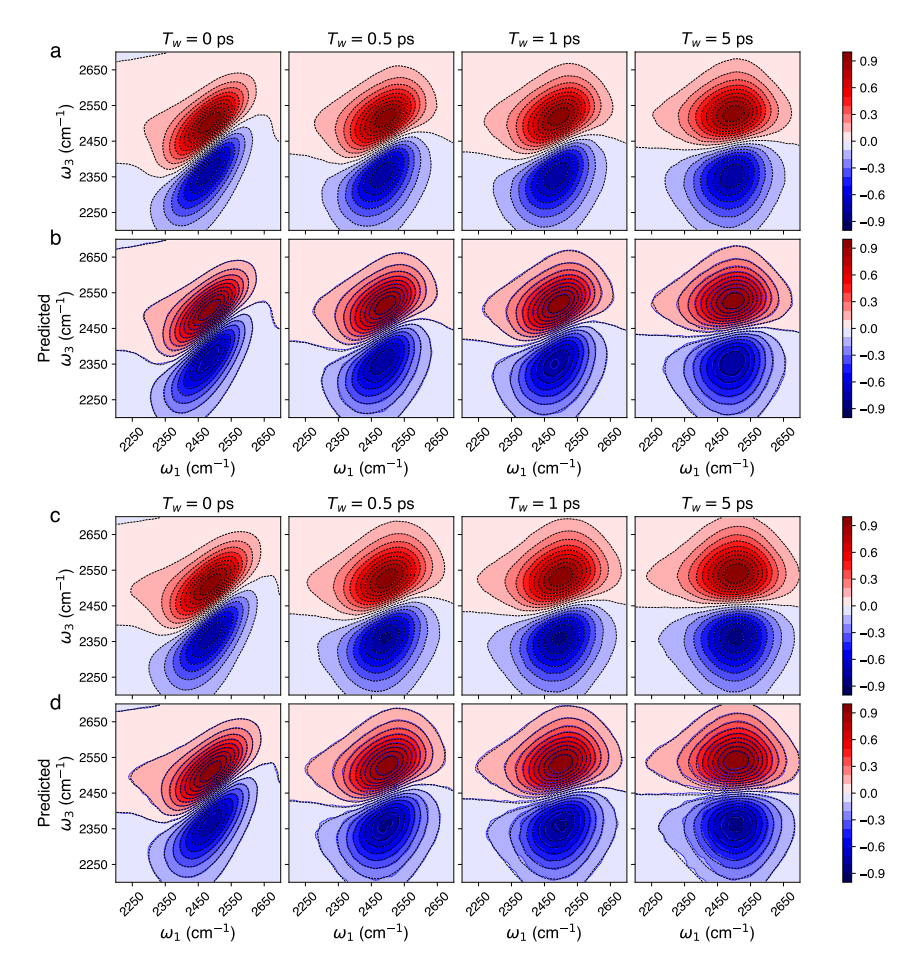


FIG. 8: a. Simulated OD stretch 2D-IR spectra of 8 M urea in HOD/H₂O at 280 K. b. First-order Taylor series prediction of the same spectra at 280 K from the 298.15 K simulations. c. Simulated OD stretch 2D-IR spectra of 8 M urea in HOD/H₂O at 320 K. d. First-order Taylor series prediction of the same spectra at 320 K from the 298.15 K simulations. Each spectrum is normalized so that its maximum equals one. Black dashed lines indicate the simulated 2D-IR spectra contours and blue dashed lines indicate the predicted 2D-IR spectra contours.

at 340 K are compared and the shortcomings are more clearly seen. Thus, it remains to develop a van't Hoff approach analogous to that previously used for the linear IR spectrum, ^{16,17} which is both a more global description and is capable of describing the changes in the peak maxima with temperature.

VI. CONCLUSIONS

We have introduced a method for directly calculating the temperature derivative of the 2D-IR spectrum from simulations at a single temperature and applied it to the case of aqueous urea solutions of varying concentration using the OD stretch of isotopically dilute water. The derivatives of both the linear IR and 2D-IR spectra are more sensitive to the urea concentration than the spectra themselves. Because the derivative is a measure of the energetic driving forces determining the spectrum, this suggests that there is significant energy-entropy compen-

sation that mutes the effect of urea on the spectra. These results thus suggest caution in drawing conclusions from examination of the spectra alone. We are unaware of any measurements of the 2D-IR spectrum of aqueous urea solutions as a function of temperature. However, the observations in this work should motivate experimental studies of the temperature dependence of 2D-IR spectra, for both the present system and others, to obtain greater insight into the driving forces of the spectral features.

As urea is added, the overall magnitude of the derivative decreases. This is similar to what was observed previously for the IR spectra when alkali-halide salts are added.¹⁷ This behavior appears to be independent of where the added solute(s) falls in terms of Hofmeister behavior, e.g., it is found for both KF, which is "structure-making" as well as urea and the other sodiumhalides, which are all "structure-breaking." ¹⁷ In the case of alkali-halide solution, we have found that, for both the diffusion coefficient and the linear IR spectra, the Hofmeister trends are determined in large part by en-

tropic factors,^{17,55} which are, however, more difficult to quantify. It will be interesting to compare the behavior of urea to other osmolytes (as well as salts), especially those that fall on the opposite end of the Hofmeister-type ranking.

Interestingly, the derivative is larger in magnitude than for the linear IR spectrum and it grows with waiting time. The method allows the decomposition of the derivative into contributions from different kinds of motions and interactions present in the system. This approach reveals a competition between the Coulombic and Lennard-Jones interaction contributions, which appears to be a universal feature of water behavior. The kinetic energy contribution is substantially larger for the 2D-IR spectrum than the linear IR spectrum.

Examination of the components of the temperature derivative associated with the different intermolecular interactions (i.e., water-water, water-urea, and urea-urea, reveals that the water-water and water-urea contributions are opposed from those due to the urea-urea ones. The water-water interactions are the largest component, but a significant contribution is found for water-urea interactions and these two appear to be the main driving force of the temperature-induced changes to the 2D-IR spectra.

We demonstrated that the derivative can be used to predict the 2D-IR spectrum at other temperatures using a simple first-order Taylor series approximation. This approach works well for a reasonable temperature range (at least $280-320~\mathrm{K}$), but improved methods are needed that provide a more universal description in the spirit of a van't Hoff approximation and enable prediction of the changes in peak heights of the spectra with temperature.

The method presented here is simple and easily implemented. The results show that it is promising, not only for determining the temperature dependence of the spectra, but for elucidating the driving forces that determine the spectra. A key element of this is the ability to decompose the temperature derivative into contributions from different interactions present in the system, and providing information that is not available in any other way.

SUPPLEMENTARY MATERIAL

See the supplementary material for force field, simulation, and empirical spectroscopic map parameters as well as center-line slope data, energetic decomposition of the IR spectra temperature derivatives, and 2D IR derivative results for 1 and 4 M urea solutions.

ACKNOWLEDGMENTS

This work was supported by the National Science Foundation under Grant CHE-2102656. N.I.C. gratefully acknowledges support from NSF REU site Grant CHE-1950293. A.K.B. gratefully acknowledges support

from a University of Kansas Dean's Doctoral Fellowship. The calculations were performed at the University of Kansas Center for Research Computing (CRC), including including the BigJay cluster resource funded through NSF Grant MRI-2117449.

DATA AVAILABILITY

The data that support the findings of this study are available from the corresponding author upon reasonable request.

APPENDIX: 2D-IR TIME CORRELATION FUNCTIONS AND DERIVATIVES

Here we present the TCFs not given in Sec. II C, that are used to calculate the 2D-IR spectrum through Eqs. (12)-(14). Each is a four-time TCF of transition dipole moments with transition frequency-determined phases and a vibrational relaxation factor. The first three contributions determine the rephasing TCF in Eq. (13) and are given by,

$$R_2(t_1, T_w, t_3) = R_1(t_1, T_w, t_3), (21)$$

and

$$R_{3}(t_{1}, T_{w}, t_{3}) = -\left\langle \mu_{01}(0) \,\mu_{01}(t_{1}) \,\mu_{12}(t_{1} + T_{w}) \right.$$

$$\mu_{12}(t_{1} + T_{w} + t_{3}) \,e^{\int_{0}^{t_{1}} \,\omega_{01}(\tau)d\tau}$$

$$e^{-\int_{t_{1}+T_{w}}^{t_{1}+T_{w}+t_{3}} \,\omega_{12}(\tau)d\tau} \right\rangle \,e^{-T_{w}/T_{1}}. \quad (22)$$

We note that the transition dipole moments have a direction and the 2D-IR measurements are typically made with particular polarization combinations that affect the components used in these expressions. In the present work we average the three terms that have the same polarization $(\hat{x}, \hat{y}, \text{ or } \hat{z})$ for all four transition dipole moments. Other polarization conditions are easily implemented.

The last three TCFs,

$$R_4(t_1, T_w, t_3) = \left\langle \mu_{01}(0) \,\mu_{01}(t_1) \,\mu_{01}(t_1 + T_w) \right.$$

$$\left. \mu_{01}(t_1 + T_w + t_3) \,e^{-\int_0^{t_1} \omega_{01}(\tau)d\tau} \right.$$

$$\left. e^{-\int_{t_1 + T_w}^{t_1 + T_w + t_3} \omega_{01}(\tau)d\tau} \right\rangle \,e^{-T_w/T_1}, \quad (23)$$

$$R_5(t_1, T_w, t_3) = R_4(t_1, T_w, t_3),$$
 (24)

and

$$R_{6}(t_{1}, T_{w}, t_{3}) = -\left\langle \mu_{01}(0) \,\mu_{01}(t_{1}) \,\mu_{12}(t_{1} + T_{w}) \right.$$

$$\mu_{12}(t_{1} + T_{w} + t_{3}) \,e^{-\int_{0}^{t_{1}} \omega_{01}(\tau)d\tau}$$

$$e^{-\int_{t_{1} + T_{w}}^{t_{1} + T_{w} + t_{3}} \omega_{12}(\tau)d\tau} \right\rangle e^{-T_{w}/T_{1}}. \quad (25)$$

give the non-rephasing contribution to the spectrum through Eq. (14). Note that these expressions, following Ref. 64, neglect vibrational lifetime effects during the t_1 and t_3 periods, an approximation based on the rapid decay of the response functions with respect those timescales.

The derivatives of these TCFs with respect to β can be expressed in terms of new TCFs defined as

$$R_{j,H}(t_1, T_w, t_3) \equiv -\frac{\partial R_j(t_1, T_w, t_3)}{\partial \beta}, \qquad (26)$$

as indicated in Eq. (16). The remaining five TCF derivatives are given by

$$R_{2,H}(t_1, T_w, t_3) = R_{1,H}(t_1, T_w, t_3), \tag{27}$$

and

$$R_{3,H}(t_1, T_w, t_3) = -\left\langle \delta H(0) \,\mu_{01}(0) \,\mu_{01}(t_1) \,\mu_{12}(t_1 + T_w) \right.$$

$$\mu_{12}(t_1 + T_w + t_3) \,e^{\int_0^{t_1} \omega_{01}(\tau)d\tau}$$

$$e^{-\int_{t_1 + T_w}^{t_1 + T_w + t_3} \omega_{12}(\tau)d\tau} \right\rangle \,e^{-T_w/T_1}, \quad (28)$$

for the rephasing contributions and

$$R_{4,H}(t_1, T_w, t_3) = \left\langle \delta H(0) \,\mu_{01}(0) \,\mu_{01}(t_1) \,\mu_{01}(t_1 + T_w) \right.$$

$$\left. \mu_{01}(t_1 + T_w + t_3) \,e^{-\int_0^{t_1} \omega_{01}(\tau)d\tau} \right.$$

$$\left. e^{-\int_{t_1 + T_w}^{t_1 + T_w + t_3} \omega_{01}(\tau)d\tau} \right\rangle e^{-T_w/T_1}, \quad (29)$$

$$R_{5,H}(t_1, T_w, t_3) = R_{4,H}(t_1, T_w, t_3), \tag{30}$$

and

$$R_{6,H}(t_1, T_w, t_3) = -\left\langle \delta H(0) \,\mu_{01}(0) \,\mu_{01}(t_1) \,\mu_{12}(t_1 + T_w) \right.$$

$$\left. \mu_{12}(t_1 + T_w + t_3) \,e^{-\int_0^{t_1} \omega_{01}(\tau)d\tau} \right.$$

$$\left. e^{-\int_{t_1 + T_w}^{t_1 + T_w + t_3} \omega_{12}(\tau)d\tau} \right\rangle e^{-T_w/T_1}. \quad (31)$$

for the non-rephasing TCFs.

- ¹P. Hamm, M. Lim, and R. M. Hochstrasser, "Structure of the Amide I Band of Peptides Measured by Femtosecond Nonlinear-Infrared Spectroscopy," J. Phys. Chem. B **102**, 6123–6138 (1998).
- ²P. Hamm and M. T. Zanni, Concepts and Methods of 2D Infrared Spectroscopy (Cambridge University Press, Cambridge, 2011).
- ³M. D. Fayer, "Dynamics of liquids, molecules, and proteins measured with ultrafast 2D IR vibrational echo chemical exchange spectroscopy," Annu. Rev. Phys. Chem. **60**, 21–38 (2009).
- ⁴S. T. Roberts, K. Ramasesha, and A. Tokmakoff, "Structural rearrangements in water viewed through two-dimensional infrared spectroscopy," Acc. Chem. Res. **42**, 1239–1249 (2009).
- ⁵N. T. Hunt, "2D-IR spectroscopy: Ultrafast insights into biomolecule structure and function," Chem. Soc. Rev. **38**, 1837–1848 (2009).
- ⁶H. J. Bakker and J. L. Skinner, "Vibrational spectroscopy as a probe of structure and dynamics in liquid water," Chem. Rev. **110**, 1498–1517 (2010).

- ⁷M. Reppert and A. Tokmakoff, "Computational amide I 2D IR spectroscopy as a probe of protein structure and dynamics," Annu. Rev. Phys. Chem. 67, 359–386 (2016).
- ⁸C. T. Kuhs, B. M. Luther, and A. T. Krummel, "Recent advances in 2D IR spectroscopy driven by advances in ultrafast technology," IEEE J. Sel. Top. Quantum Electron. 25, 3100313 (2019).
- ⁹K. S. Maiti, "Two-dimensional infrared spectroscopy reveals better insights of structure and dynamics of protein," Molecules 26, 6893 (2021).
- ¹⁰D. Kraemer, M. L. Cowan, A. Paarmann, N. Huse, E. T. Nibbering, T. Elsaesser, and R. J. Dwayne Miller, "Temperature dependence of the two-dimensional infrared spectrum of liquid H₂O," Proc. Natl. Acad. Sci. U. S. A. **105**, 437–442 (2008).
- ¹¹R. A. Nicodemus, K. Ramasesha, S. T. Roberts, and A. Tok-makoff, "Hydrogen bond rearrangements in water probed with temperature-dependent 2D IR," J. Phys. Chem. Lett. 1, 1068–1072 (2010).
- ¹²R. A. Nicodemus, S. A. Corcelli, J. L. Skinner, and A. Tok-makoff, "Collective hydrogen bond reorganization in water studied with temperature-dependent ultrafast infrared spectroscopy," J. Phys. Chem. B **115**, 5604–5616 (2011).
- ¹³F. Perakis and P. Hamm, "Two-dimensional infrared spectroscopy of supercooled water," J. Phys. Chem. B **115**, 5289–5293 (2011).
- ¹⁴O. O. Mesele and W. H. Thompson, "Removing the barrier to the calculation of activation energies," J. Chem. Phys. **145**, 134107 (2016).
- ¹⁵Z. A. Piskulich, O. O. Mesele, and W. H. Thompson, "Activation energies and beyond," J. Phys. Chem. A 123, 7185–7194 (2019).
- ¹⁶Z. A. Piskulich and W. Thompson, "Temperature dependence of the water infrared spectrum: Driving forces, isosbestic points, and predictions," J. Phys. Chem. Lett. 11, 7762–7768 (2020).
- ¹⁷A. K. Borkowski and W. H. Thompson, "Shining (infrared) light on the hofmeister series: Driving forces for changes in the water vibrational spectra in alkali-halide salt solutions," J. Chem. Phys. B 126, 6700–6712 (2022).
- ¹⁸P. H. Yancey, "Water stress, osmolytes and proteins," Amer. Zool. 41, 699–709 (2001).
- ¹⁹P. H. Yancey, "Organic osmolytes as compatible, metabolic and counteracting cytoprotectants in high osmolarity and other stresses," J. Exp. Biol. **208**, 2819–2830 (2005).
- ²⁰W. J. Xie, S. Cha, T. Ohto, W. Mizukami, Y. Mao, M. Wagner, M. Bonn, J. Hunger, and Y. Nagata, "Large hydrogen-bond mismatch between TMAO and urea promotes their hydrophobic association," Chem. 4, 2615–2627 (2018).
- ²¹S. G. Zetterholm, G. A. Verville, L. Boutwell, C. Boland, J. C. Prather, J. Bethea, J. Cauley, K. E. Warren, S. A. Smith, D. H. Magers, and N. I. Hammer, "Noncovalent interactions between trimethylamine N-oxide (TMAO), urea, and water," J. Phys. Chem. B 122, 8805–8811 (2018).
- ²²M. Mukherjee and J. Mondal, "Bottom-up view of the mechanism of action of protein-stabilizing osmolytes," J. Phys. Chem. B **124**, 11316–11323 (2020).
- ²³C. J. Sahle, M. A. Schroer, J. Niskanen, M. Elbers, C. M. Jeffries, and C. Sternemann, "Hydration in aqueous osmolyte solutions: The case of TMAO and urea," Phys. Chem. Chem. Phys. 22, 11614–11624 (2020).
- ²⁴J. K. Carr, L. E. Buchanan, J. R. Schmidt, M. T. Zanni, and J. L. Skinner, "Structure and dynamics of urea/water mixtures investigated by vibrational spectroscopy and molecular dynamics simulation," J. Phys. Chem. B 117, 13291–13300 (2013).
- ²⁵D. Bandyopadhyay, S. Mohan, S. K. Ghosh, and N. Choudhury, "Molecular dynamics simulation of aqueous urea solution: Is urea a structure breaker?" J. Phys. Chem. B 118, 11757–11768 (2014).
- ²⁶Y.-T. Liao, A. C. Manson, M. R. DeLyser, W. G. Noid, and P. S. Cremer, "Trimethylamine N-oxide stabilizes proteins via a distinct mechanism compared with betaine and glycine," Proc. Natl. Acad. Sci. 114, 2479–2484 (2017).
- ²⁷M. Auton and D. W. Bolen, "Predicting the energetics of

- osmolyte-induced protein folding/unfolding," Proc. Natl. Acad. Sci. **102**, 15065–15068 (2005).
- ²⁸D. W. Bolen and G. D. Rose, "Structure and energetics of the hydrogen-bonded backbone in protein folding," Annu. Rev. Biochem. 77, 339–362 (2008).
- ²⁹S. Lee, Y. L. Shek, and T. V. Chalikian, "Ureas interactions with protein groups: A volumetric study," Biopolymers **93**, 866–879 (2010).
- ³⁰M. C. Stumpe and H. Grubmüller, "Interaction of urea with amino acids: Implications for urea-induced protein denaturation," J. Am. Chem. Soc. **129**, 16126–16131 (2007).
- ³¹E. J. Guinn, L. M. Pegram, M. W. Capp, M. N. Pollock, and M. T. Record Jr., "Quantifying why urea is a protein denaturant, whereas glycine betaine is a protein stabilizer," Proc. Natl. Acad. Sci. 108, 16932–16937 (2011).
- ³²L. B. Sagle, Y. Zhang, V. A. Litosh, X. Chen, Y. Cho, and P. S. Cremer, "Investigating the hydrogen-bonding model of urea denaturation," J. Am. Chem. Soc. 131, 9304–9310 (2009).
- ³³S. Micciulla, J. Michalowsky, M. A. Schroer, C. Holm, R. von Klitzinga, and J. Smiatek, "Concentration dependent effects of urea binding to poly(N-isopropylacrylamide) brushes: a combined experimental and numerical study," Phys. Chem. Chem. Phys. 18, 5324–5335 (2016).
- ³⁴B. J. Bennion and V. Daggett, "The molecular basis for the chemical denaturation of proteins by urea," Proc. Natl. Acad. Sci. **100**, 5142–5147 (2003).
- ³⁵K. A. Sharp, B. Madan, E. Manas, and J. M. Vanderkooi, "Water structure changes induced by hydrophobic and polar solutes revealed by simulations and infrared spectroscopy," J. Chem. Phys. 114, 1791–1796 (2001).
- ³⁶J. Grdadolnika and Y. Marećhal, "Urea and urea-water solutions An infrared study," J. Mol. Struct. **615**, 177–189 (2002).
- ³⁷A. K. Soper, E. W. Castner, and A. Luzar, "Impact of urea on water structure: a clue to its properties as a denaturant?" Biophys. Chem. **105**, 649–666 (2003).
- ³⁸Y. L. Rezus and H. J. Bakker, "Effect of urea on the structural dynamics of water," Proc. Natl. Acad. Sci. U. S. A. **103**, 18417– 18420 (2006).
- ³⁹C. J. Sahle, M. A. Schroer, I. Juurinend, and J. Niskanen, "Influence of TMAO and urea on the structure of water studied by inelastic X-ray scattering," Phys. Chem. Chem. Phys. 18, 16518 (2016).
- ⁴⁰D. Ojha and A. Chandra, "Urea in water: Structure, dynamics, and vibrational echo spectroscopy from first-principles simulations," J. Phys. Chem. B **123**, 3325–3336 (2019).
- ⁴¹W. H. Brandeburgo, S. T. van der Post, E. J. Meijerab, and B. Ensing, "On the slowdown mechanism of water dynamics around small amphiphiles," Phys. Chem. Chem. Phys. 17, 24968 (2015).
- ⁴²B. Lovrinčević, M. Požar, and M. Balić, "Dynamics of urea-water mixtures studied by molecular dynamics simulation," J. Mol. Liq. 300, 27–31 (2020).
- ⁴³K. R. Harris, R. Mills, P. J. Back, and D. S. Webster, "An improved NMR spin-echo apparatus for the measurement of self-diffusion coefficients: The diffusion of water in aqueous electrolyte solutions," Biophys. J. 29, 473–482 (1978).
- ⁴⁴K. D. Collins and M. W. Washabaugh, "The Hofmeister effect and the behaviour of water at interfaces," Q. Rev. Biophys. 18, 323–422 (1985).
- ⁴⁵J. D. Smith, R. J. Saykally, and P. L. Geissler, "The effects of dissolved halide anions on hydrogen bonding in liquid water," J. Am. Chem. Soc. **129**, 13847–13856 (2007).
- ⁴⁶H. Ohtaki and T. Radnai, "Structure and dynamics of hydrated ions," Chem. Rev. 93, 1157–1204 (1993).
- ⁴⁷H. J. Bakker, "Structural dynamics of aqueous salt solutions," Chem. Rev. **108**, 1456–1473 (2008).
- ⁴⁸Y. Marcus, "Effect of ions on the structure of water: Structure making and breaking," Chem. Rev. **109**, 1346–1370 (2009).
- ⁴⁹Y. Zhang and P. S. Cremer, "Chemistry of Hofmeister anions and osmolytes," Annu. Rev. Phys. Chem. 61, 63–83 (2010).

- ⁵⁰Y. Okazaki, T. Taniuchi, G. Mogami, N. Matubayasi, and M. Suzuki, "Comparative study on the properties of hydration water of Na- and K-halide ions by Raman OH/OD-stretching spectroscopy and dielectric relaxation data," J. Phys. Chem. A 118, 2922–2930 (2014).
- ⁵¹W. J. Xie and Y. Q. Gao, "A simple theory for the Hofmeister series," J. Phys. Chem. Lett. 4, 4247–4252 (2013).
- ⁵²K. I. Assaf and W. M. Nau, "The chaotropic effect as an assembly motif in chemistry," Angew. Chem. Int. Ed. **57**, 13968–13981 (2018).
- ⁵³R. Zangi, "Can salting-in/salting-out ions be classified as chaotropes/kosmotropes?" J. Phys. Chem. B **114**, 643–650 (2010).
- ⁵⁴J. S. Kim, Z. Wu, A. R. Morrow, A. Yethiraj, and A. Yethiraj, "Self-diffusion and viscosity in electrolyte solutions," J. Phys. Chem. B **116**, 12007–12013 (2012).
- ⁵⁵A. K. Borkowski, Z. A. Piskulich, and W. H. Thompson, "Examining the Hofmeister series through activation energies: Water diffusion in aqueous alkali-halide solutions," J. Chem. Phys. B 125, 350–359 (2021).
- ⁵⁶H. S. Frank and F. Franks, "Structural approach to the solvent power of water for hydrocarbons; Urea as a structure breaker," J. Chem. Phys. 48, 4746–4757 (1968).
- ⁵⁷K. Yoshida, K. Ibuki, and M. Ueno, "Pressure and temperature effects on ²H spin-lattice relaxation times and ¹H chemical shifts in *tert*-butyl alcohol- and urea-D₂O solutions," J. Chem. Phys. **108**, 1360–1367 (1998).
- ⁵⁸H. Lee, J.-H. Choi, P. K. Verma, and M. Cho, "Computational vibrational spectroscopy of HDO in osmolyte-water solutions," J. Phys. Chem. A **120**, 5874–5886 (2016).
- ⁵⁹D. Laage, G. Stirnemann, F. Sterpone, R. Rey, and J. T. Hynes, "Reorientation and allied dynamics in water and aqueous solutions," Annu. Rev. Phys. Chem. **62**, 395–416 (2011).
- ⁶⁰R. F. Greene and H. B. Callen, "On the formalism of thermodynamic fluctuation theory," Phys. Rev. 83, 1231–1235 (1951).
- ⁶¹T. L. Hill, Statistical Mechanics. Principles and Selected Applications (Dover, New York, 1956).
- ⁶²K. J. Tielrooij, C. Petersen, Y. L. Rezus, and H. J. Bakker, "Reorientation of HDO in liquid H₂O at different temperatures: Comparison of first and second order correlation functions," Chem. Phys. Lett. **471**, 71–74 (2009).
- ⁶³ J. R. Schmidt, S. A. Corcelli, and J. L. Skinner, "Pronounced non-Condon effects in the ultrafast infrared spectroscopy of water," J. Chem. Phys. **123**, 044513 (2005).
- ⁶⁴S. M. Gruenbaum, P. A. Pieniazek, and J. L. Skinner, "Vibrational spectroscopy of water in hydrated lipid multi-bilayers. II. Two-dimensional infrared and peak shift observables within different theoretical approximations," J. Chem. Phys. 135, 164506 (2011).
- $^{65} \mbox{The}$ LAMMPS molecular dynamics package, http://lammps.sandia.gov (downloaded July 8, 2020).
- ⁶⁶S. Plimpton, "Fast parallel algorithms for short-range molecular dynamics," J. Comput. Phys. 117, 1–19 (1995).
- ⁶⁷H. J. C. Berendsen, J. R. Grigera, and T. P. Straatsma, "The missing term in effective pair potentials," J. Phys. Chem. 91, 6269–6271 (1987).
- ⁶⁸S. Weerasinghe and P. E. Smith, "A Kirkwood-Buff derived force field for mixtures of urea and water," J. Phys. Chem. B **107**, 3891–3898 (2003).
- ⁶⁹D. P. Shoemaker, C. W. Garland, and J. W. Nibler, Experiments in Physical Chemistry (McGraw-Hill, New York, 1989).
- ⁷⁰S. A. Corcelli, C. P. Lawrence, and J. L. Skinner, "Combined electronic structure/molecular dynamics approach for ultrafast infrared spectroscopy of dilute HOD in liquid H₂O and D₂O," J. Chem. Phys. **120**, 8107–8117 (2004).
- 71 S. A. Corcelli and J. L. Skinner, "Infrared and Raman line shapes of dilute HOD in liquid H₂O and D₂O from 10 to 90 $^{\circ}$ C," J. Phys. Chem. A **109**, 6154–6165 (2005).
- ⁷²B. Auer, R. Kumar, J. R. Schmidt, and J. L. Skinner, "Hydrogen bonding and Raman, IR, and 2D-IR spectroscopy of dilute HOD

- in liquid D₂O," Proc. Natl. Acad. Sci. **104**, 14215–14220 (2007).
- ⁷³S. M. Gruenbaum, C. J. Tainter, L. Shi, and J. L. Skinner, "Robustness of frequency, transition dipole, and coupling maps for water vibrational spectroscopy," J. Chem. Theory Comput. 9, 3109–3117 (2013).
- ⁷⁴K. Kwak, D. E. Rosenfeld, and M. D. Fayer, "Taking apart the two-dimensional infrared vibrational echo spectra: More information and elimination of distortions," J. Chem. Phys. **128**, 204505 (2008).
- ⁷⁵Z. A. Piskulich, O. O. Mesele, and W. H. Thompson, "Removing the barrier to the calculation of activation energies: Diffusion coefficients and reorientation times in liquid water," J. Chem. Phys. 147, 134103 (2017).
- ⁷⁶Z. A. Piskulich and W. H. Thompson, "Examining the role of different molecular interactions on activation energies and activation volumes in liquid water," J. Chem. Theory Comput. 17, 2659–2671 (2021).

- ⁷⁷Z. A. Piskulich and W. H. Thompson, "The activation energy for water reorientation differs between IR pump-probe and NMR measurements," J. Chem. Phys. **149**, 164504 (2018).
- ⁷⁸Z. A. Piskulich, D. Laage, and W. H. Thompson, "Activation energies and the extended jump model: How temperature affects reorientation and hydrogen-bond exchange dynamics in water," J. Chem. Phys. **153**, 074110 (2020).
- ⁷⁹Z. A. Piskulich and W. H. Thompson, "On the temperature dependence of liquid structure," J. Chem. Phys. **152**, 011102 (2020).
- ⁸⁰C. H. Mendis, Z. A. Piskulich, and W. H. Thompson, "Tests of the Stokes-Einstein relation through the shear viscosity activation energy of water," J. Phys. Chem. B 123, 5857–5865 (2019).
- ⁸¹Z. A. Piskulich, D. Laage, and W. H. Thompson, "On the role of hydrogen-bond exchanges in the spectral diffusion of water," J. Chem. Phys. **154**, 064501 (2021).